Received: 2 January 2023 | Accepted: 12 June 2023

DOI: 10.1111/1365-2478.13389

Geophysical Prospecting | EAGE EUROPEAN ASSOCIATION OF GEOSCIENTISTS & ENGINEERS

ORIGINAL ARTICLE

# A workflow for processing mono-channel Chirp and Boomer surveys

**Aldo Vesnaver** | **Luca Baradello**

National Institute of Oceanography and Applied Geophysics – OGS, Sgonico, Italy

**Correspondence**
Aldo Vesnaver, National Institute of Oceanography and Applied Geophysics – OGS, Sgonico, Italy.
Email: avesnaver@ogs.it

**Abstract**

Acquiring seismic data with multichannel, multiple-streamer and even multi-componentsystems at sea provides excellent images of the Earth. However, the cost and complexity of operations prevent their use in busy areas such as ports or in sensitive environments such as lagoons. In the latter cases, mono-channel Chirp or Boomer systems are the most viable instruments for marine surveys. The lack of multiple offsets prevents the use of standard tools for amplitude-versus-offset and velocity analysis, which are necessary for the lithological characterization of rocks, especially for the shallow sediments in offshore engineering. In this paper, we present a few recent techniques that exploit the traveltime and amplitude of multiple reflections to compensate for the offset limitation, including a new algorithm for the joint tomographic inversion of direct arrivals, primaries and multiples. We have developed a cost-effective workflow for mono-channel surveys based on a data-driven, physically consistent philosophy that attempts to approximately extract lithological parameters, such as P velocity, anelastic absorption, acoustic impedance and even density. We applied the proposed workflow to a real field experiment and obtained a semi-quantitative estimate for shallow sediments that can be used by offshore engineers.

KEYWORDS
acquisition, inversion, seismics, signal processing, tomography

## INTRODUCTION

In recent decades, seismic data acquisition and processing have made spectacular progress, thanks to massive investments by the oil and gas industry in the development of new technologies. Following the 3D seismic revolution of the last century, the number of channels in acquisition systems has skyrocketed (Pecholcs et al., 2010, 2012), and sophisticated processing methods such as full-waveform inversion (Alkhalifah, 2014; Plessix, 2008, among many others) have consolidated. Thus, multi-parameter Earth models can be estimated with increasing resolution and reliability (Huang et al., 2018). However, the expected long-term decline in oil and gas exploration and production due to the planned energy transition to mitigate global warming is leading to a decline in public and private investment in this area. Therefore, the existing hydrocarbon detection technology should be shifted to other geosciences, such as hydrology and geoengineering. This paper presents some recent and new seafloor characterization algorithms for marine geology and offshore engineering. These tools can greatly improve the information obtained by very low-cost surveys, such as mono-channel Chirp or Boomer profiles (Müller et al., 2002, 2009). These marine high-resolution methods use a temporary-long (up

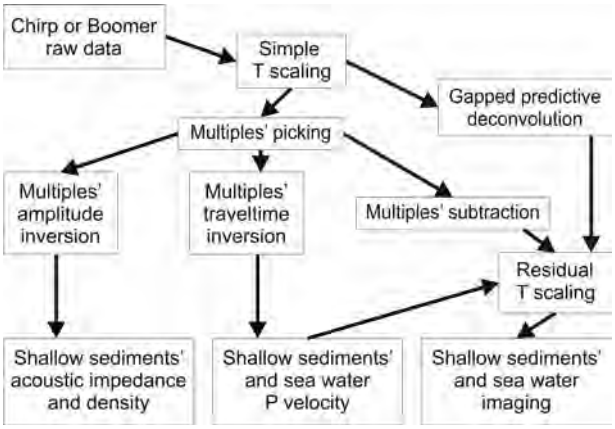


**FIGURE 1** Proposed workflow for processing Chirp and Boomer mono-channel data.

to 32 ms), frequency-modulated source-waveform (Gutowski et al., 2002; Schock & LeBlanc, 1990) and a temporally short (<1 ms) impulsive source-waveform (McGee, 1995; Verbeek & McGee, 1995), respectively. These systems are far inferior to multichannel and multi-streamer systems in terms of inversion and imaging quality (Hite & Fontana, 2007; Landais et al., 2014; Moldoveanu et al., 2020), but they may be the best option in busy areas such as harbours (Barsottelli-Botelho & Mesquita, 2015) or sensitive protected areas, such as marine reserves (Gordon et al., 2003), lagoons (Zecchin et al., 2008) or even archeological sites (Müller et al., 2009). Bull et al. (1998) modelled the seafloor reflectivity to detect a wreck using the polarity of uncorrelated Chirp data. The standard processing flow applied to the mono-channel high-resolution seismic (including Boomer and Sparker) and Chirp data comprises simple steps, such as automatic gain control, time-varying frequency filters and predictive deconvolution (Alves & Mahiques 2019; Duchesne & Bellefleur 2007).

In this paper, we present a processing flow that follows the data and physical criteria as much as possible, trying to overcome the strict limitations of a single-channel acquisition system. Adopting data-driven algorithms, we reduce the work required to the interpreter and also the related personal bias. Figure 1 shows the main steps, which are described in detail in the following sections and then applied to real examples. We start with the raw field data and take special care not to apply any adaptive gain function (such as automatic gain control or normalizations by maximum or average amplitude). Otherwise, the information from the lateral and vertical variations of the signal amplitude would be destroyed. With algorithms based on the simplified physics of a 1D Earth model, we can use the amplitude and traveltimes of multiples to compensate to some extent for the lack of receiver multiplicity. In this way, we obtain a semi-quantitative estimate of the P velocity, acoustic impedance and density of shallow marine sediments. The uncertainties in the estimation are not negligible, but they can be very useful for practical applications when the alternative can only be expensive and invasive exploratory drilling.

In the first section, we address compensation for the geometrical spreading, which is a challenge if we ignore (at least initially) the Earth's velocity model. In the second section, we present a simple method for subtracting multiples: once applied, the correction for geometrical spreading can be further adjusted based on the data, accounting for anelastic absorption to some extent. We show that a conventional deconvolution method such as gapped predictive deconvolution is theoretically suitable not only for Boomer surveys but also for the Chirp data. After improving the amplitude fidelity of the signal, we show in the third section that we can use the amplitude of the multiples to invert the reflectivity and acoustic impedance of the seafloor. To get an indication of the density of the shallow sediments, we need to estimate their P velocity: In the fourth section, we show that this information can be obtained by joint tomographic inversion of primary signals and some multiples types. A final section is devoted to the detection of fluid plumes in seawater for marine geological studies.

## GEOMETRICAL SPREADING CORRECTION

To use the information about the Earth in the signal amplitude, we must first compensate for its geometrical spreading. The seismic energy is distributed on wave fronts that expand and propagate in the rock layers as a function of time and local velocity: therefore, in principle, each event should be corrected by its own spreading factor, according to a 3D velocity model. However, for single-channel data, the uncertainty of the estimated velocity can be substantial, especially at small distances between source and receiver (Vesnaver & Baradello, 2022a). The only signals we can confidently deal with are the multiples reverberating between the seafloor and the surface. The velocity of seawater can be estimated by independent measurements of temperature and salinity using an empirical formula (Mackenzie, 1981). In most cases, a value of 1500 m/s is a good approximation, although reported experimental values range from 1430 to 1520 m/s. Vesnaver et al. (2003) suggested that local and seasonal variations should be taken into account and that seawater velocity should be set as a variable parameter to be estimated at each location during the survey.

The total energy $E_0$ of an ideal instantaneous pulse over a spherical wavefront of radius $r_0$ is equal to $4\pi\, {r_0}^2\, {a_0}^2$, where $a_0$ is the signal amplitude at time $t_0$. In an elastic medium, the energy remains constant during the propagation, and so at a time $t$ the energy is $E(t) = 4\pi\, r(t)^2\, a(t)^2 = E_0$. As a

consequence, we get:

$$a_1(t) = a_0 r_0 / r(t) = a_0 r_0 / \left(v_w t\right), \quad (1)$$

where $v_w$ is the velocity of the seawater. The amplitude decay $a_1(t)$ of a pulse over time $t$ is inversely proportional to its distance $r$ from the emitting source when propagating in an elastic homogeneous 3D medium.

Multiplying each value in a seismogram $s(t)$ by a factor $v_w\, t$, the amplitudes of the seafloor reflection and its multiples are compensated for the decay that occurs in a 1D Earth model for a plane wave perpendicular to horizontal layers. We will see in a later section that this is necessary for both removing and inverting the multiples.

The function $a_1(t)$ holds for a source emitting seismic pulses isotropically in the seawater. This assumption is a fair approximation for Chirp systems or Boomer with a single plate – (as for the data presented in this paper, with a diameter of 40 cm). Boomers with a plate array have an anisotropic radiation pattern focused along the vertical direction (Crocker & Frantantonio, 2016). This pattern may be characterized by the angle $\varphi$ between the orthogonal to the sea surface and the line where the signal amplitude is half of its maximum. Ruppel et al. (2022) showed that this angle is about 60° for a three-plate directional Boomer. In similar cases, the isotropic factor $a_1(t)$ can produce an over-compensation and should be modified allowing for the $\varphi$ angle.

Claerbout (1985) and Denich et al. (2021) have shown that an additional factor $t^{-1}$ should be added in the signal compensation if we assume that the source spectrum is white and the propagation medium is homogeneous but anelastic. In this hypothesis, a different $a_2(t)$ compensation function should be used:

$$a_2(t) = 1/(at), \quad (2)$$

where $\alpha$ is the anelastic absorption coefficient of the medium. Such a function may enhance the primaries fairly but overemphasize the multiples. An intermediate effect is obtained if a non-white (and thus more realistic) source spectrum is considered. Based on an exercise proposed by Claerbout (1985), Denich et al. (2021) proved that the function $a_\beta(t)$ is a good approximation:

$$a_\beta(t) = \Gamma(\beta+1)/(at)^{\beta+1}, \quad (3)$$

where $\Gamma(.)$ is the Gamma function and $\beta$ is the exponent of the function $|\omega|^\beta$ that best fits the amplitude spectrum of the source, where $\omega$ is the angular frequency. Relation (3) is valid for $\beta > -1$ and allows to compensate only the anelastic absorption contribution. Either (2) or (3) should be applied in sequence after the factor $a_1(t)$, so that the cumulative exponent for the time $t$ becomes 2 or $2 + \beta$. The $\beta$ parameter must be negative, otherwise, the function $|\omega|^\beta$ would diverge. Values for $\beta$ close to $-0.5$ are quite common for Chirp or Boomer data according to our practical experience.

## A REAL DATA-SET

To test the proposed workflow and highlight its intermediate steps, we selected a Boomer survey acquired in the port of Trieste (Adriatic Sea). This geophysical survey was requested for a possible extension of about 200 m of the Trieste Marine Terminal, to improve the commercial traffic capability. The port of Trieste has a deep natural draft of about 18 m, which is very attractive for the modern high-capacity vessels. The port is protected by artificial breakwaters, making the water surface definitely calm. During the acquisition, no boat or vessel could navigate close to the straight line of the profile. In the bay, the sediment consists of Holocene marine muddy deposits up to 10 m thick, overlying the Late Pleistocene fluvial channel-levee system that crossed the bay during the subaerial exposure of the last glacial period (Trobec et al., 2018). The inflow of fresh water in the port is negligible, as proven by the high salinity in the whole Gulf of Trieste.

The system type is an electrodynamic plate AAE301, with a sampling interval of 50 μs and a recording duration of 200 ms. The plate is mounted on a catamaran frame, suspended at a constant depth of 10 cm to reduce dragging turbulence. The actual offset is ranging from 3 to 3.5 m, with a mono-channel receiver composed of an array of 8 preamplified hydrophones. The shooting interval is three times per second, corresponding to 0.6–0.7 m in space, due to the normal navigation speed of 3.5–4 kn. The water depth is about 15 m along the profile, which is parallel to the coastline. The streamer with the receiver is kept as shallow as possible (i.e. a few cm) with suitable floaters to avoid the possible destructive interference produced by the air–water interface. The price paid for this advantage is an increase of the noise due to the sea waves, which we reduced later by a low-cut filtering.

The depth source is about 30 cm on catamaran and its nominal source frequency ranges from 100 to 7000 Hz. A low-cut filter was applied to eliminate the ultra-low frequency that normally affects this type of data, due to spurious currents. The sea conditions were good during the acquisition, so not affecting the data quality.

## APPLICATION EXAMPLE

Our first processing step was a simple band-pass Ormsby filter with corner frequencies of 100, 1000, 5000 and 7000 Hz to remove the very low-frequency noise that is typical of Boomer surveys, which is very strong in our case too. Figure 2

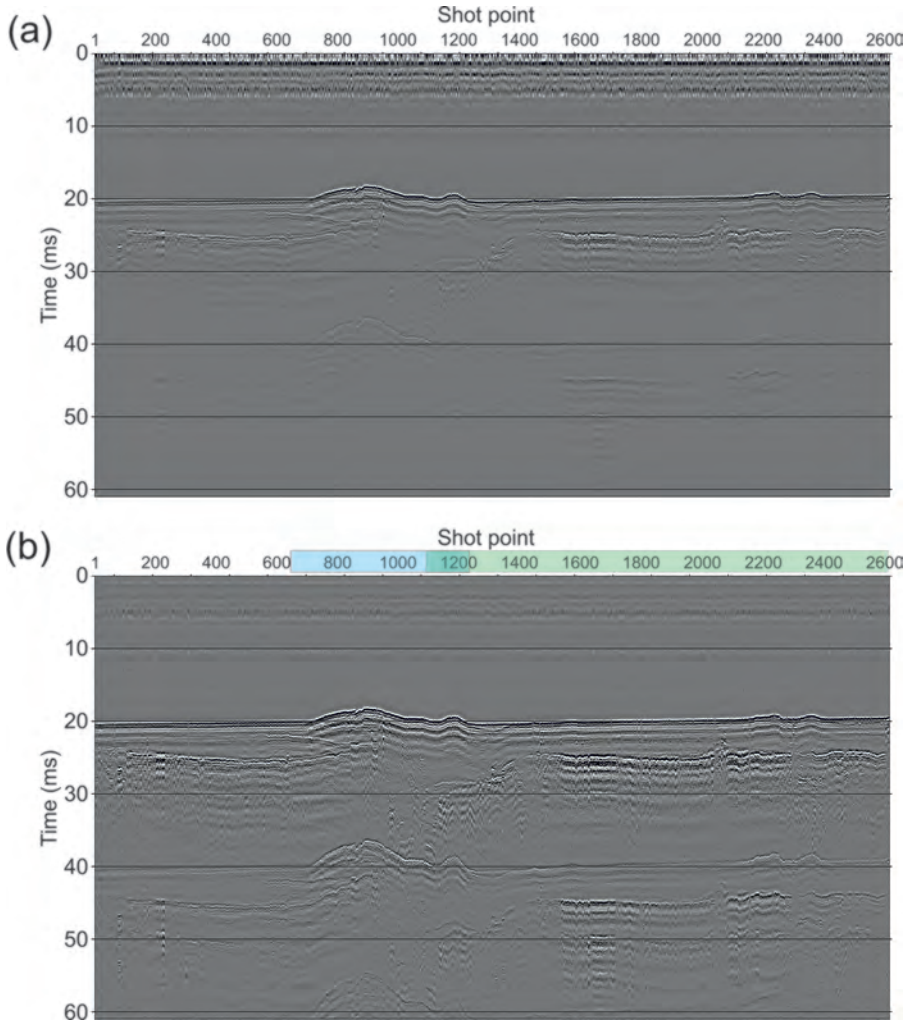


**FIGURE 2** Seismic sections with the Boomer data after a preliminary band-pass filtering, without (a) and with (b) a geometrical spreading correction using the functions $a_1(t)$ for the propagation in the seawater only (b). The blue rectangle indicates the shot range used later for the amplitude inversion, and the green one shows that one used for the traveltime tomography.

shows the profile before and after the correction for the propagation in the water layer, that is using the function $a_1(t)$. In the plot, a global equalization was carried out to compare the two seismic sections, while preserving the lateral amplitude variations due to a different reflectivity. We notice that the multiples' train duplicating the seafloor between 40 and 60 ms is stronger, although its amplitude is not so high as the primary.

In addition to a sharper image of primaries (around 20 ms) and multiples (around 40 ms), we notice also some weak shallow events between 0 and 5 ms. The earliest ones are direct arrivals from the source to the streamer, with an offset between source and receiver of about 3 m. As the source depth is 30 cm only, a possible ghost contribution becomes part of the main signal. The other arrivals just below it should be reflections from different water layers, due to some sharp change in the water temperature at a depth of a couple of meters. These and other arrivals above the sea floor are normally muted out, but we will see later that they may bear important information.

Figure 3a displays the autocorrelation of the data in Figure 2b, that is after the compensation for the geometrical spreading. The very first peak may be due to a ghost effect of source and receiver: as both are at a depth of 30 cm, the corresponding two-way traveltime is 0.4 ms for a seawater velocity of 1500 m/s. At a short lag, that is about 5 ms, we notice the peaks due to reverberations in the shallow sediments. At lags of about 20 ms we see the peaks due to seafloor multiples, which account for most of the energy. At later times, weaker peaks correspond to higher-order multiples. In the amplitude spectra (Figure 3b), we notice that most of the signal energy ranges from 1000 to 6000 Hz, as we removed the lowest frequencies that are dominated by noise.

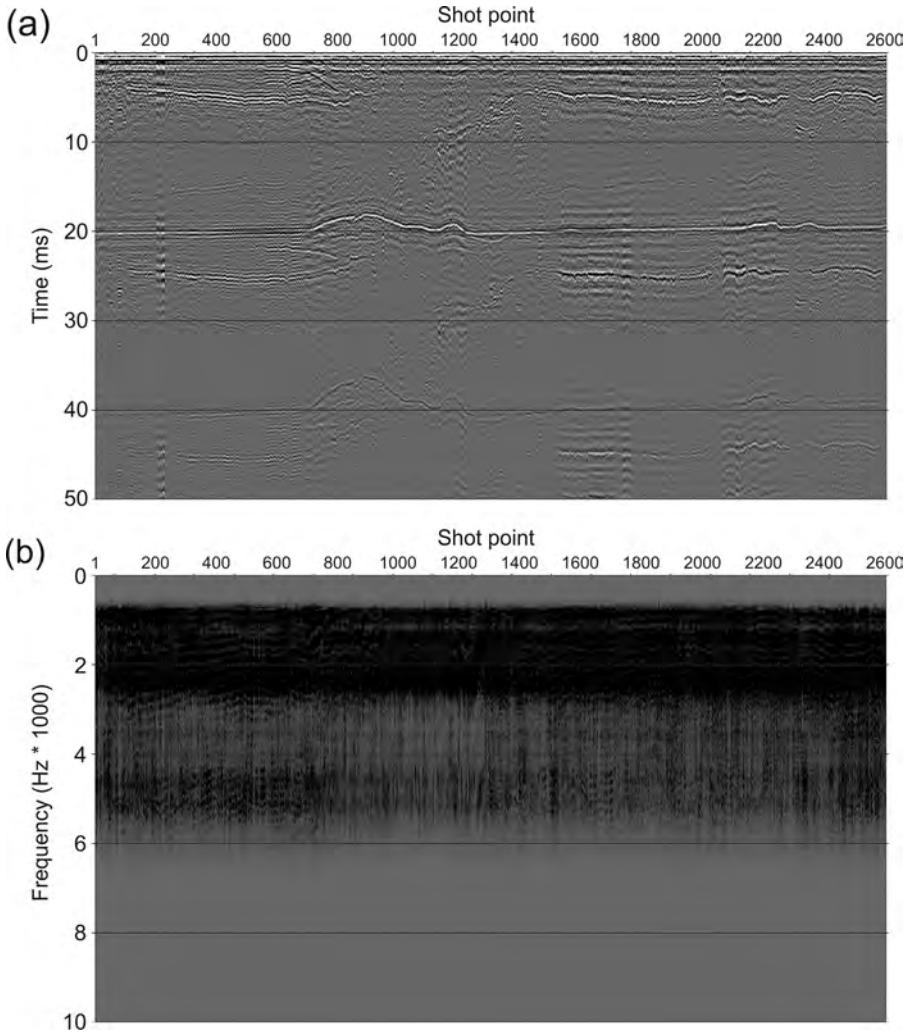


**FIGURE 3** Autocorrelation (a) and amplitude spectra (b) of the data in Figure 2b.

## MULTIPLES' ATTENUATION

For Chirp or Boomer surveys in shallow waters, multiple reflections from the seafloor are a major problem because their strength can overwhelm weaker reflections from shallow sediments. Mono-channel surveys cannot rely on established methods, such as SRME (surface-related multiple elimination) (Verschuur et al., 1992), Tau-p domain deconvolution (Russell et al., 1990) or FK filtering (Yilmaz, 2001, among others) that exploit the redundancy and geometry of multiple offsets. The simplest solution is to return to good old predictive deconvolution (Peacock & Treitel, 1969; Robinson & Treitel, 1967), using a prediction distance that is close to the two-way traveltime between the seafloor and the surface. This algorithm, also referred to as gapped deconvolution, is certainly applicable to Boomer surveys because this impulsive source produces waveforms that closely resemble minimum-phase wavelets. Some doubts may arise when dealing with conventional Chirp data. The Chirp source emits short sweeps that, after a cross-correlation, become pulses like the Boomer. The standard recording system immediately converts the received signal to its envelope; otherwise, the narrowband high-frequency signal is very difficult to interpret. Recently, however, Denich et al. (2021) proved a theorem stating that the envelope of a minimum-phase wavelet is still a minimum-phase wavelet. On this basis, applying a gapped deconvolution to enveloped Chirp traces is a mathematically correct option, if the original Chirp signal is converted to minimum-phase.

Figure 4a displays the image obtained by a gapped deconvolution, using a prediction distance of 16 ms and a filter length of 19 ms. In this way, the filter acts mainly to the multiples, which are indeed attenuated a lot. We note only a few traces affected by numerical ringing. In the time range of multiples, between 40 and 60 ms, we cannot distinguish other clear primaries, although a few low-frequency scattered signals show up that do not seem to be multiple residuals.

Another classical approach to multiple attenuation is its modelling and subtraction (see, e.g. Fomel, 2009; Wiggins, 1988). We picked the seafloor traveltime semi-automatically

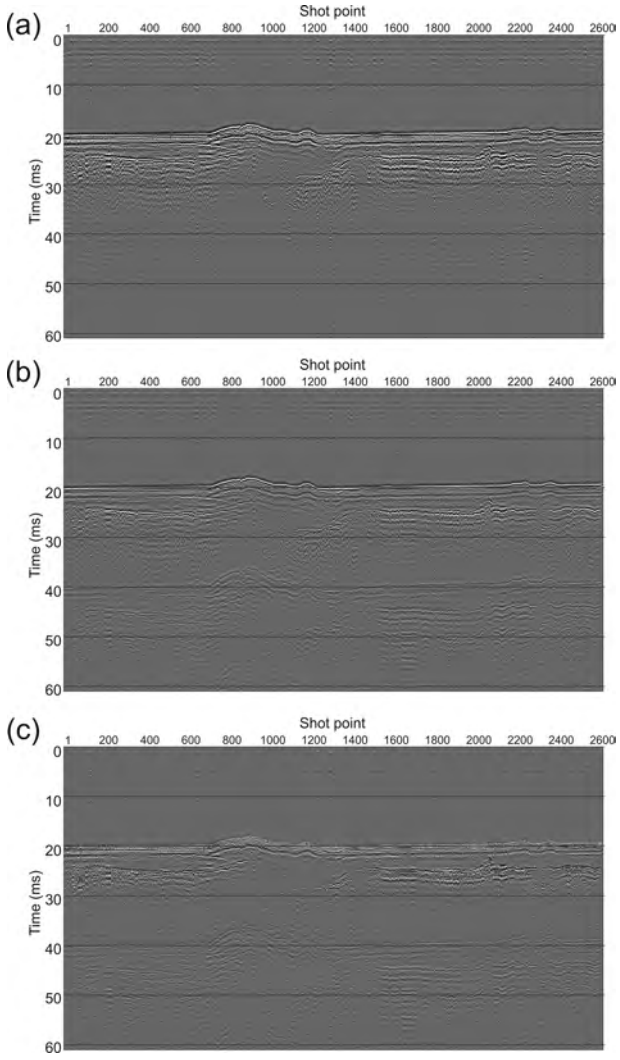


**FIGURE 4** Multiple attenuation by gapped deconvolution (a) and multiple subtraction (b) applied to the data in Figure 2. These sections are normalized by their average energy. Their difference (c) is computed as a plain subtraction of (a) and (b).

by cross-correlating the seafloor reflections with a pilot wavelet. We then extracted a time window that started at the seafloor and included all reflections up to the first multiple arrival time. We aligned this window of events by maximizing the coherence between shifted primaries and their multiples, scaled by a factor that minimized the resulting energy. For more details, we refer the reader to Vesnaver et al. (2021).

Figure 4b shows how this approach compares with gapped deconvolution. In our case, it is a bit less effective in mitigating the multiples but preserves nicely the relative amplitude differences in the shallow sediments. The shallowest reflectors are sharper and show lateral variations in reflectivity, so contributing to interpretations based on seismic stratigraphy. On the other hand, when dealing with Chirp data, this approach introduces negative values are that are not expected in a normal Chirp section. They can simply be set to zero if a standard display of Chirp data is preferred.

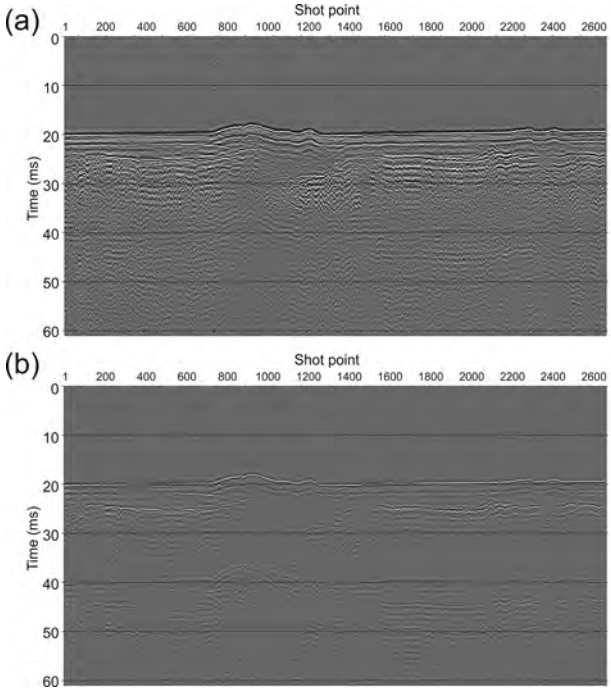


**FIGURE 5** Multiple attenuation by gapped deconvolution (a) and multiple subtraction (b) applied to the data in Figure 2, multiplied by the data-driven function $a_\beta(t)$, using a $\beta$ value of $-0.35$ and $-0.395$, respectively. The sections are normalized by their average energy.

Figure 4c highlights the results obtained by these methods for multiple attenuation, computed by a plain difference between the two sections normalized by their energy. A residual multiple is evident between 40 and 50 ms, but even higher differences show up at the see floor around 20 ms, due to the ringing introduced by predictive deconvolution. The latter one is more effective for attenuating multiples, but the price paid is a distortion of the reflectivity in the shallow sediments.

According to the workflow in Figure 1, the next step is compensating for the amplitude decay due to the anelastic absorption in the formations below the seafloor. We computed different values for the $\beta$ coefficient fitting the average amplitude spectra of the two entire sections in Figure 5, that is $-0.35$ for the gapped deconvolution and $-0.395$ for the multiple subtraction. This difference depends on the diverse amplitudes of the multiple residuals. We cannot detect new signals below the attenuated multiples, but we get minor improvements in the imaging of shallow reflectors.

## REFLECTIVITY AND DENSITY FROM MULTIPLES

Picking of the primary reflection from the seafloor and its shallow multiples is tedious and challenging, and sometimes impossible if the signal is overlaid with noise. However,

this processing step allows inverting the amplitudes of these signals to estimate the seafloor reflectivity.

Figure 6 shows the typical multiples that we can expect in a shallow marine survey: what we call 'simple', that is with two reflections at a layer interface and one at the sea surface; a peg-leg multiple, that is a primary reflection from the base of sediments followed by a bounce in the water layer; an intrabed multiple, including a bounce in the sediment layer; and reverberations in the water layer between the sea floor and surface. We plotted the direct arrival too, which may be used in Boomer surveys for controlling the actual offset between source and receiver. Among the multiples, the amplitude of the reverberations in the water layer allows estimating the reflectivity of the seafloor.

If the offset between the source and the receiver is small (e.g. 3 m) and the seafloor is flat, we can approximate the Earth with an acoustic 1D model that assumes vertical propagation of seismic waves in seawater. After compensating for the geometrical spreading by (1), the amplitude of the reverberating signals depends only on the initial value $S$ at the source, the reflection coefficient $R_0$ at the air–water contact at the sea surface and the reflection coefficient $R_1$ of the seafloor. The amplitude $A_j$ of the signal recorded at the sea surface after $j$ bounces through the water layer is

$$A_j = S\, R_1^j R_0^{(j-1)}. \tag{4}$$

where $A_1$ refers to the primary reflection, $A_2$ to its first multiple and so on. For P velocities of 343 and 1500 m/s for air and seawater, respectively, and corresponding densities of 1.225 and 997 kg/m$^3$, the reflection coefficient $R_0$ at the sea surface is 0.9994, which can be approximately expressed as 1. Since the relation (4) holds for any integer value of $j$, we can replace $j$ with $(j + 1)$ and obtain:

$$A_{j+1} = S\, R_1^{(j+1)}\, R_0^j. \tag{5}$$

Dividing (5) by (4), we get:

$$A_{j+1}/A_j = R_0 R_1 \approx R_1. \tag{6}$$

Thus, the amplitude ratio of two successive bounces does not depend on the source strength $S$, but only on the reflection coefficients $R_0$ and $R_1$ at the water layer boundaries. If we approximate $R_0$ by 1, these ratios depend only on the seafloor reflectivity $R_1$. When sea waves cause a rough surface, the reflectivity can change and become even frequency-dependent, in principle. However, Chapman and Scott (1964) showed experimentally that this effect is negligible for small offsets and for acoustic sources with frequency ranging from 100 to 6400 Hz.

In principle, many multiples can appear in our records, but because of random noise and interference with other events, in most cases, we can only detect the seafloor reflection and its first two multiples. To estimate $R_1$ from the measured amplitudes $A_j$, we can define and minimize an object function $O(A_j)$:

$$O\left(A_j\right) = \sum \left(\bar{A}_j - A_j\right)^2 = O\left(S, R_0, R_1\right), \tag{7}$$

where $\overline{A_j}$ are the measured amplitudes and $A_j$ are values modelled by (4) by testing different values for $S$, $R_0$ and $R_1$. When $R_0$ is set to 1, only two terms are needed in (7), which otherwise becomes an overdetermined system. However, our experience with noisy data has shown that the three-terms function in (7) gives more stable results. Further improvements can be achieved by writing the relation (6) explicitly for the first and second multiple:

$$A_2/A_1 = R_0 R_1 = A_3/A_2, \tag{8}$$

and rearranging it as

$$A_2^2 - A_1 A_3 = 0. \tag{9}$$

Equation (9) can be used as a constraint for minimizing (7). Deviations of the experimental data from this relationship can measure the signal level with respect to noise.

An alternative algorithm for solving (4) is taking the logarithm side by side. As an example, for $j$ ranging from 1 to 3, we get a system of 3 equations in 3 unknowns, which is simpler and faster to be computed. However, this approach cannot reduce the deviations from the physical constraints expressed by (9) due to the random noise in the data.

Theoretically, we can go one step further. The reflectivity $R_1$ for offsets close to zero depends on the acoustic impedance of the shallow sediments $\rho_{\text{sed}}\, v_{\text{sed}}$ and that of the seawater $\rho_{\text{w}}\, v_{\text{w}}$:

$$R_1 = (\rho_{\text{sed}} v_{sed} - \rho_{\text{w}} v_{\text{w}})/(\rho_{\text{sed}} v_{\text{sed}} + \rho_{\text{w}} v_{\text{w}}), \tag{10}$$

where $\rho_{\text{sed}}$ and $\rho_{\text{w}}$ are the densities, and $v_{\text{sed}}$ and $v_{\text{w}}$ are the velocities of the two media. Rearranging (10), we obtain:

$$\rho_{\text{sed}} v_{\text{sed}} = \rho_{\text{w}} v_{\text{w}} \frac{1 + R_1}{1 - R_1}. \tag{11}$$

For deep waters, the density $\rho_{\text{w}}$ and velocity $v_{\text{w}}$ of seawater can be estimated by measuring the temperature and salinity during the survey, using the formulas of Millero et al. (1980) and Mackenzie (1981), among others. In shallow waters these formulas may not hold, and so a direct measurement of water velocity and density may be needed. In the next section, we will see that we can also estimate the sediment velocity $v_{\text{sed}}$ by exploiting the multiples' traveltimes. In this way, all terms in

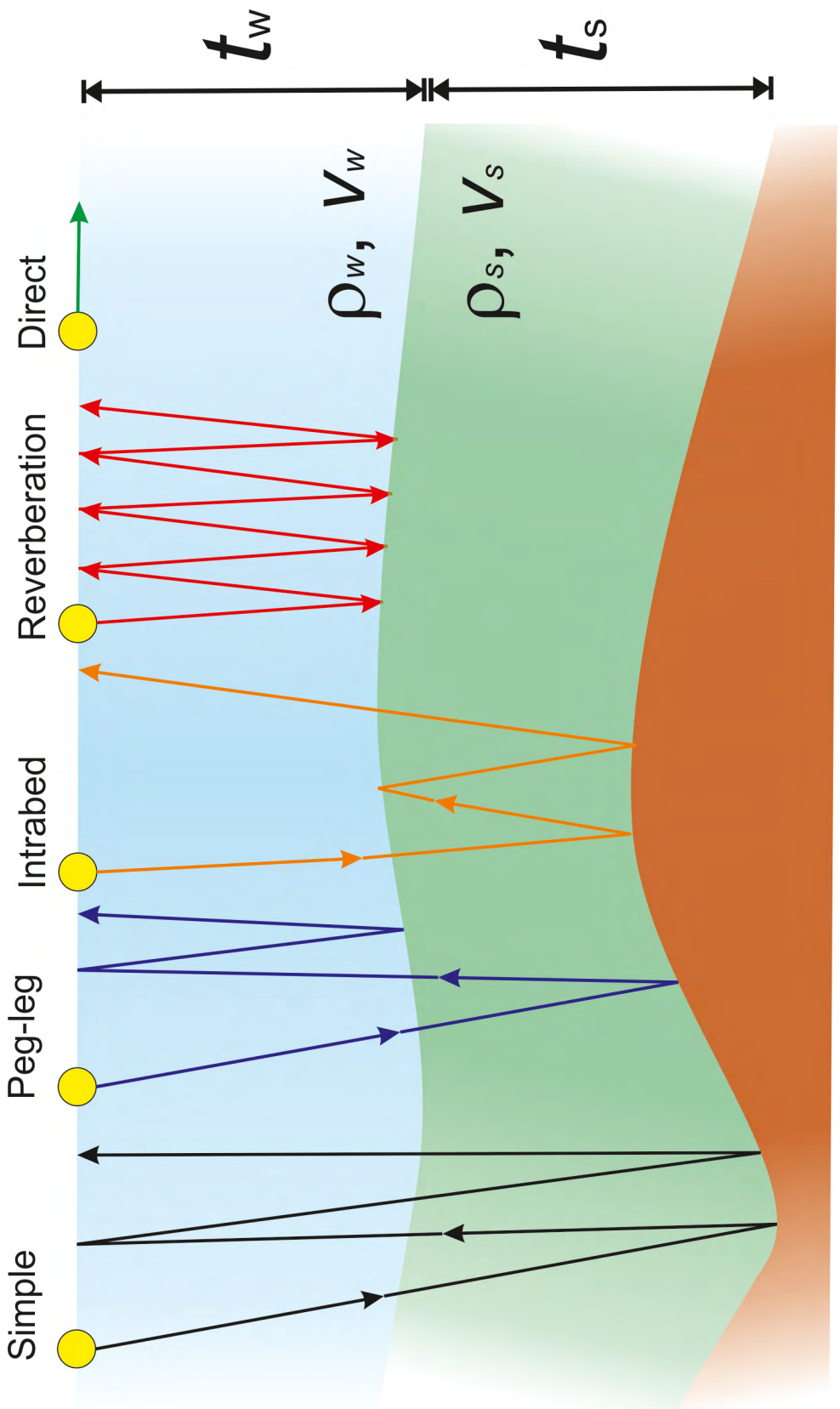


**FIGURE 6** A quasi-1D Earth model composed of a water layer over a layer of sediments, overlying a half-space. The ray paths of different multiple types are sketched in the cartoon, from left to right: simple (black line), peg-leg (blue line), intrabed multiples (orange line) and reverberations in the water layer (red line). The direct arrival (green line) is shown too.

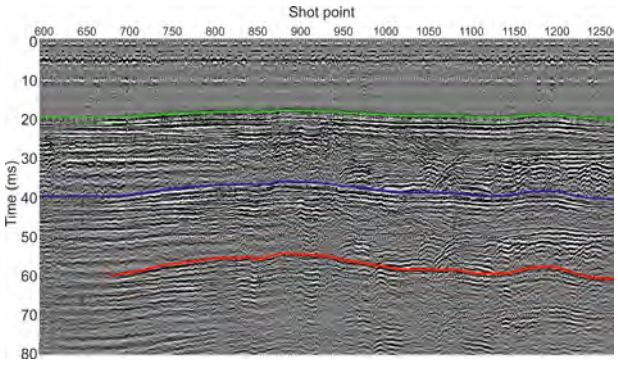


**FIGURE 7** Picked primary reflection from the seafloor (green line), first simple multiple (blue line) and second simple multiple (red line) of the part of the section indicated by a blue rectangle in Figure 2.

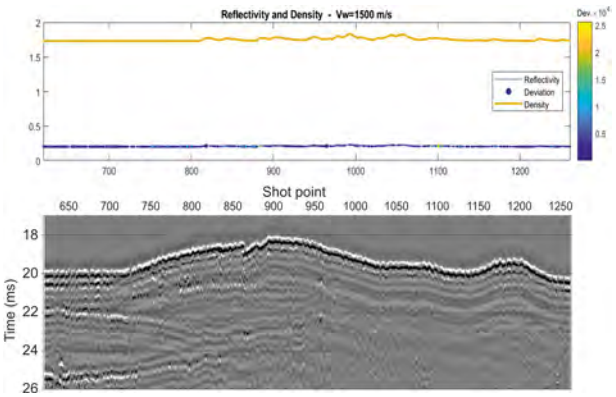


**FIGURE 8** Estimated reflectivity (blue line), reflectivity reliability measured by the deviation (coloured dots) and density (yellow line) estimated using a sediment velocity of 1250 m/s, superimposed to a zoom of the seafloor reflection and the shallowest underlying signals.

(11) become available except for the density $\rho_{sed}$, which can thus be calculated by solving this equation.

Figure 7 shows the picked primary reflection of the seafloor (green line) and its simple multiples (blue and red lines). We skipped events too weak or uncertain, to avoid compromising the inversion quality. The seafloor is slightly curved upwards and very smooth, except for a small irregularity close to the shot 850. This irregularity is a good guide for detecting and picking the first and second simple multiples.

The picking procedure is different between Boomer signals (which are minimum-phase) and Chirp signals (which are zero-phase). For the latter ones, the traveltime at the maximum amplitude of the waveform must be selected. For Boomer signals, instead, the first onset of the waveform must be picked: this is normally easy for the seafloor primary, but quite challenging for the multiples. Moreover, we must allow for the polarity reversal occurring at each reflection backwards from the sea surface. Trying to optimize the picking quality, we tested two ways: a first one was just a careful manual picking of the signal onset, and a second one was the maximum (or minimum) amplitude of the waveform followed by a time correction. We computed its amount by estimating an average signal wavelet over the main reflections of the whole section, measuring the traveltime difference between the waveform onset and its maximum. The two approaches, however, produced very similar results and require comparable efforts, so we can hardly recommend either of the two.

For the inversion of the amplitudes, we assumed a standard seawater velocity of 1500 m/s. Figure 8 shows the estimated reflectivity (blue line), which is nearly constant, ranging from 0.20 to 0.22. This smoothness fits the visual impression we get when we look at the underlying magnified details of the corresponding seismic traces. The coloured dots superimposed on the reflectivity line are mostly blue, indicating minimal deviations from the fit expressed by Equation (9). The yellow line is the estimated density assuming an average sediment velocity of 1250 m/s. This value may seem too low, since it is lower than the velocity of seawater, but we will see in the next section that this value approximates the tomographic estimates. The density values range from 1.73 to 1.82 g/cm$^3$, which is consistent with the sandy sediments present in the area. The density curve is slightly oscillating at the seafloor irregularities but does not fit tightly their traveltime variations as well as might be expected for an independent lithologic parameter.

As the sea floor is quite flat in our case, the signal amplitude dependance on the source directivity is negligible. When the sea floor dip is significant, instead, some compensation is necessary. For frequency at the lower side of Chirp sources, for example 2000 Hz, the amplitude decreases by 3 dB at an angle of 60°, and 6 dB at 90°. At frequencies around 8000 Hz, the signal vanishes at 60°. For Boomer plates, Riedel and Theilen (2001) showed that similar dependencies exist. The compensation for the source directivity is critical for AVO (amplitude versus offset) analysis of multichannel surveys, which is not possible for mono-channel seismic data.

## VELOCITY ESTIMATION BY MULTIPLES AND PRIMARIES

Velocity analysis with multichannel recording systems uses the time difference for the same reflected event at different offsets between source and receivers. Algorithms range from simple stacking velocity analysis (Maine, 1962; Taner & Koehler, 1969) to migration velocity scans (see, e.g. Biondi, 2006; Yilmaz, 2001) to the most advanced full-waveform inversion methods (Alkhalifah, 2014; Plessix, 2008), which may even incorporate artificial intelligence (Alkhalifah et al., 2021). Single-channel systems lack this information redundancy. For Boomer and Chirp systems, only a single offset is available, which is small (for Boomers) or simply zero (for

Chirps): in other words, these surveys provide a common-offset or even just a zero-offset gather. When diffractions are present, post-stack time-domain migration velocity scans can in principle give an indication of velocity, but the uncertainty for such an approach can be substantial (Fomel et al., 2007). In this paper, we propose instead a tomographic approach that takes advantage of the redundancy of information added to the primaries by the traveltimes of the multiples.

A few multiple types occur frequently in shallow marine surveys. The easiest to detect, and often the strongest, is the first-order multiple, which comes from the seafloor and bounces only once on the sea surface, which we call a 'simple multiple'. Occasionally, second- or third-order multiples of similar type can also be reliably detected: in this case, their amplitude inversion can provide information about the lithology of shallow sediments. Another common type is a peg-leg multiple, that is a deeper primary wave followed by a bounce of the seismic waves in the water layer. The most difficult type to interpret is intrabed multiples, which occur as reverberations within two strong deep horizons: they are weaker and possible irregularities of these horizons complicate their pattern recognition. Figure 6 shows a cartoon with examples of these multiples in a simple quasi-1D model, that is with small lateral variations, consisting of two layers, the seawater and the shallow sediments, over a half-space. For better illustration, we have highlighted the thickness variations and the offset between source and receiver, which are much smaller in reality. In the remainder of this section, we assume that this is our Earth model, although more layers could be considered. For most engineering applications, the properties of the shallow sediments are the key information sought.

In a tomographic Earth model such as the one in Figure 6, the water depth can be determined directly from the primary reflection of the seafloor, provided the seawater velocity is known. Then two parameters must be estimated: the thickness and velocity of shallow sediments. At least two measurements are required for two unknowns: one is the primary reflection from the base of the sediments, and the second can be any multiple type, that is single, peg-leg or intrabed. If more types are available at the same location, so much the better: the tomographic system of equations will be overdetermined, but usually this condition improves solution stability in terms of noise and reduces the contribution of null space (van der Sluis & van der Vorst, 1987; Vesnaver, 1994).

A tomographic estimate of the velocity $v_s$ and thickness $t_s$ of the sediments is obtained by minimizing the object function $M(v_s, t_s)$ with the squared differences between observed and modelled traveltimes:

$$M\left(v_s,t_s\right) = \sum_j \left(\overline{tp_j} - tp_j\right)^2 + \sum_j \left(\overline{ts_j} - ts_j\right)^2 + \sum_j \left(\overline{tpl_j} - tpl_j\right)^2 + \sum_j \left(\overline{ti_j} - ti_j\right)^2, \quad (12)$$

where $tp_j$, $ts_j$, $tpl_j$ and $ti_j$ indicate the modelled traveltimes as a function of the test velocity $v_s$ and test thickness $t_s$, whereas the related barred terms are the picked traveltimes in the seismic traces. Of course, where there are not picked events, the corresponding difference is set to zero. The minimization of the object function (12) can be achieved by a crude exhaustive search in a pre-defined window. In our trace-by-trace approach, the size of both the data and the unknown Earth parameters is small, and so the calculation is very fast in a normal personal computer. More elegant optimization methods might be preferred, as Genetic Algorithms or Simulated Annealing, but their cost-effectiveness is questionable. A viable improvement can be expected from gradient-based algorithms, instead.

In the modelling of the traveltimes for (12), attention must be paid to the source and receiver depth, because its contribution is not negligible. As we are using the sea surface as a datum plane, we must increase the source traveltime by its depth divided by seawater velocity, which is 0.2 ms in our Boomer case study. If the receivers are floating (as in our test case), not further corrections are needed. When dealing with Chirp data, where source and receiver depth coincide, we may prefer assuming the datum plane as located at the source/receiver depth. In that case, traveltime corrections are not needed for the primary reflections, but only at each bounce of the signal to the sea surface. For more details on the modelling and inversion strategy, we refer the reader to Vesnaver and Baradello (2022a, 2022b, 2022c).

Minimization of (12) is actually 1D tomography based on a trace-by-trace inversion. The noise and mutual interference of events, especially in late multiples, lead to instabilities that can be reduced by setting limits on the lateral variations of velocity and thickness, since from a geologic point of view strong variations of these properties are rarely expected. An effective smoothing procedure is to apply a lateral median filter along the profile for both estimated velocities and thicknesses, as this removes isolated spikes while preserving sharp anomalies of significant extent.

For the inversion of amplitudes to estimate seafloor reflectivity, we chose a subset of traces in the range 620–1261 (blue bar in Figure 2) because the irregularity of the seafloor allowed us to pick two simple multiples in this range with confidence. Another range is more suitable for estimating P velocity of shallow sediments, namely the shots from 1125 to 2629 (Figure 9). Below the seafloor (green line), there is a clear discontinuity in the seismic stratigraphy (yellow line), which is slightly dipping and irregular on the left side, while it is shallower and flatter in the middle and right parts. The reflectivity of this horizon is strong and can produce a prominent peg-leg multiple (light blue line) that can be used for tomographic inversion of traveltimes in addition to the first simple multiple (dark blue line). We picked also the direct arrival (red line) to compensate for the variations in

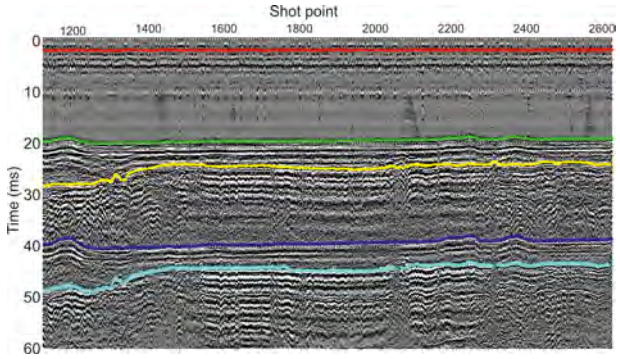


**FIGURE 9** Picked horizons used for the traveltime inversion: direct arrival (red), seafloor (green), base of shallow sediments (yellow), first simple multiple (dark blue) and peg-leg multiple (light blue).

source-receiver offset due to cable feathering and ocean waves (see, e.g. Lin et al., 2019). The latter ones may cause depth differences between source and receiver in Boomer surveys that may be not negligible if the sea is rough.

Figure 10 shows the estimated P velocity (red line) and thickness (blue line) for the shallow sediments by tomographic inversion of the events picked in Figure 9. The sediment velocity is extremely stable, with minor deviations from a mean value of 1.25 km/s, whereas the layer thickness is affected by a few spikes and minor instabilities that can be smoothed with a median filter. However, the estimate is consistent with the time section in Figure 9, as its shape is specular to the yellow horizon therein, given a nearly constant P velocity of the sediment layer. The offset between source and receiver was estimated by dividing the traveltime of the direct arrival by the assumed seawater velocity. The offset so obtained (yellow line) varies much more in percentage; however, there is no correlation with sediment velocity and thickness.

Figure 11 provides a clue about the inversion stability, by depicting the misfit being minimized as a function of layer velocity and thickness in their tested range. Except for the spike at the corner with a large thickness (3 m) and low velocity (1000 m/s), we notice an almost flat valley. This indicates that the inversion is not well posed, as minor errors in the input data may end up into much larger errors in the Earth model estimates (Vesnaver & Baradello, 2022a, 2022c).

# DISCUSSION

## Result interpretation

The sediment velocity is unexpectedly low and below the velocity of seawater. A likely explanation is the presence of gas trapped in the formation. Carcione and Poletto (2000) showed that even a low gas saturation of 1% can reduce the P velocity of water-based drilling mud from 1.6 to 1.2 km/s. Helle et al. (2003) analysed the effects of gas saturation on both velocity and anelastic absorption. Dusart et al. (2022) jointly inverted seismic and electrical measurements in an area with gas-bearing shallow sediments, getting P velocities between 1200 and 1400 m/s. Chen et al. (2023) obtained similar results for gas-saturated sands using X-ray and acoustic tomography. The ideal validation of our results would rely on seabed sampling and analysis for velocity and gas content, but this data is not available so far in this area.

Several areas populated by fluid plumes have been reported throughout the Gulf of Trieste (Busetti et al., 2010, 2013, 2020; Conti et al., 2002; Geletti et al., 2008; Gordini et al., 2012; Hovland & Curzi, 1989), and so we tested this hypothesis further. First, a velocity drop from seawater to sediments should produce a reflection with opposite polarity with respect to deeper consolidated sediments. Zooming in on the first few traces from Figure 7, we can clearly see such polarity reversal (Figure 12).

This polarity reversal is not present in the initial part of the profile (Figure 2, shot 1–700) that is not suitable for the tomographic inversion. In a central part (shot 700–1200), the layers between 20 and 30 ms are bent and fractured, and some faded possible gas chimneys show up. From these conduits, some gas can migrate in the shallower formation on the right side, infiltrating the unconsolidated sediments and being released slowly in the seawater. A continuous gas flow from the deeper sediments may end up into a dynamic equilibrium of the fluid system. Cevatoglu et al. (2015) showed that a similar phenomenon occurs in a controlled $CO_2$ injection experiment: a minor, faint gas chimney may occur in the proximity of the injection point, but the area affected by measurable seismic anomalies (as signal amplitude and anelastic absorption) is wide, due to a significant lateral migration of fluids. In Figure 2, some fault is visible while minor fractures cannot be imaged, but the tectonic compression of deeper layers is very clear in the central part. We notice a bright spot at about 25 ms on the right side, which can be a formation where the gas accumulates and is slowly released upwards towards the sea floor. This formation seems fractured, because its signal is wavy, while the overlying sea floor is very smooth. We notice finally that the signal strength is consistent with the velocity contrast between the two media, which is about 14%.

Our hypothesis is further supported when we consider the instantaneous frequency of these data, that is the derivative of the instantaneous phase (Taner et al., 1979; Vesnaver, 2017). It is proportional to the barycentre of the instantaneous spectrum (Ackroyd, 1970; Saha, 1987), and therefore its shift to lower frequencies can be used as a function of propagation time to estimate the anelastic absorption of the penetrated medium (Lin et al., 2018, 2022). This algorithm is applicable to both Boomer and non-enveloped Chirp data. In Figure 13,

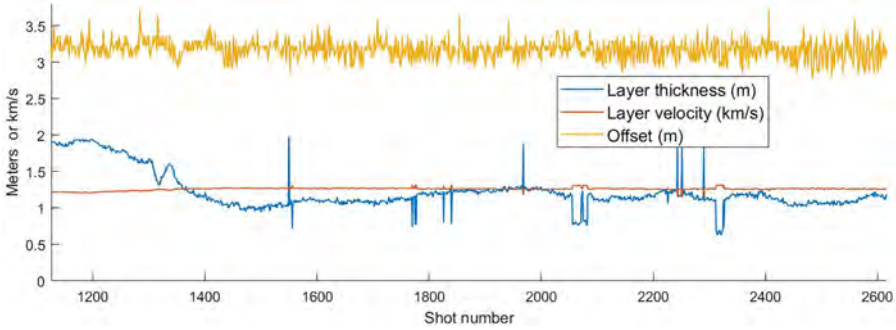


**FIGURE 10** Sediment velocity and thickness estimated for the data in Figure 9 using the traveltime joint inversion of the seafloor primary, peg-leg and the first simple multiple.

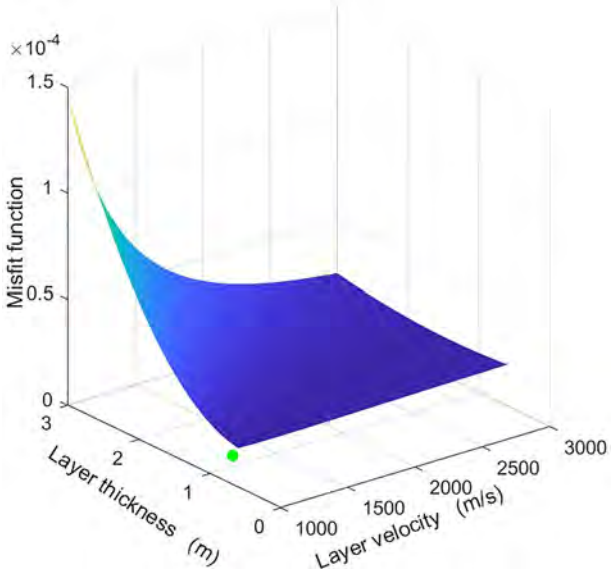


**FIGURE 11** Misfit function for a trace at the centre of the profile. The green dot is the vertical projection of the minimum misfit between measured and modelled traveltimes as a function of trial layer thickness and velocity.

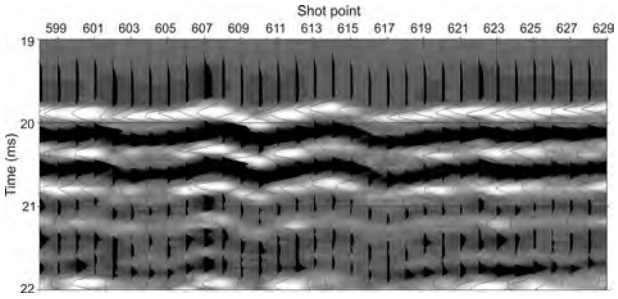


**FIGURE 12** Enlarged detail of the uppermost reflections in a few traces from Figure 7, highlighting the negative polarity of the seafloor reflection.

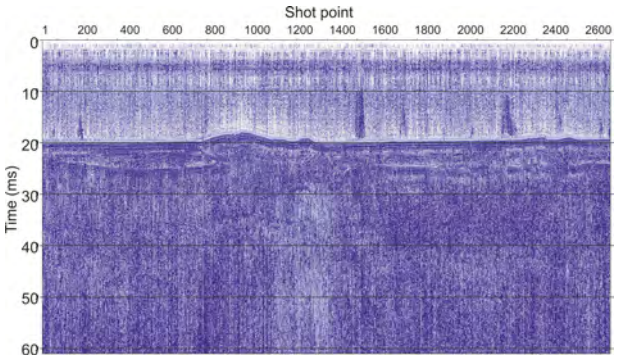


**FIGURE 13** Instantaneous frequency of the data in Figure 5a, that is after a gapped deconvolution and a compensation for geometrical spreading and anelastic absorption.

several plumes are clearly visible in the water layer throughout the profile at shot points 170, 1420, 1620, 2100 and 2560. Some of them are barely visible also in Figure 9. They could be due to the release of gas from the saturated sediments and from the underlying formations. Other hypotheses seem us weaker because of the anomalies shape: they involved several adjacent traces, so implying a lateral extension of a couple of meters at least, and mostly cover a vertical distance from the seafloor to the sea surface, occasionally disappearing when approaching the surface. These features rule out alternatives as moored buoys and are too weak to be due to rock formations or wrecks. Further measurements as seawater analysis and cores of shallow sediments could validate the proposed gas migration mechanism.

In our Earth model, we approximated the water layer by a homogeneous medium. Seawater temperature, salinity and P-wave velocity may change laterally and vertically, although these variations are often smooth. Low-frequency distortions may be so introduced in the estimated inversion parameters by this Earth simplification. Unfortunately, we cannot handle too many unknowns in our inversion algorithm because of the minimal size of the data, that is traveltimes and amplitudes of a few picked events. Future developments may move towards the full-waveform inversion: in that case, each trace sample is bearing information and mathematical constraints, so

allowing in principle a much higher resolution for both the water layer and the underlying sediments.

A lithological parameter that cannot be estimated directly by acoustic marine surveys is the S velocity of the shallow sediments, and so the shear modulus, which is important for offshore engineering. Zero- or short-offset mono-channel data cannot estimate an angle-dependent reflectivity. Another useful parameter, that is resistivity, can be jointly inverted with seismic data (Dusart et al., 2022).

A clear link between gas-bearing sediments and an increase of seabed compressibility has been reported by Sills and Wheeler (1992) and Kim et al. (2014), a decrease of permeability by Sultan et al. (2007) and an increase of resistivity by Goswami et al. (2016), among others.

## Other imaging improvements

A final polish to improve the imaging of the seismic sections is provided by various classical post-stack algorithms, such as time-domain migration, FX deconvolution and complex attributes. Only Boomer data are suitable for wave equation migration because they relate to a physical signal in the strict sense. Standard Chirp data are usually the envelope of real waveforms and as such are always non-negative. For this reason, they do not cancel when summed 'out of phase', but rather sum to a higher or lower cumulative amplitude. Artefacts occur primarily at the seafloor where there are bumps. Nevertheless, this heuristic approach can be an effective tool for reducing diffractions. Baradello (2014) has shown that migrating Chirp data before taking their envelope provides excellent images, and a similar experience is reported by Uge and Alp (2018). We therefore strongly recommend recording Chirp data in their original form and calculating their envelope later to facilitate visual interpretation. In our experience, omitted here for brevity, we have obtained good results using the phase shift method (Gazdag 1978).

FX deconvolution is not based on the wave equation, but only on the assumed statistics of the signal: it is therefore equally applicable to Boomer and Chirp data. Again, the application does not change the normal appearance of Boomer data, which contain both positive and negative peaks, but that of enveloped Chirp data, where only positive peaks are expected. This detail aside, this algorithm works very well in most cases. Ideally, it should follow the possible post-stack migration in the time domain, since the latter reduces spatially organized noise as diffractions that might otherwise be amplified by FX deconvolution. For application examples, we refer the reader to Baradello (2014), Uge and Alp (2018), Denich et al. (2021) and Vesnaver et al. (2021).

## Chirp versus Boomer data

The main processing steps of the workflow proposed in this paper apply equally to Boomer and enveloped Chirp data: spherical divergence correction, inversion of amplitudes and traveltime of multiples to estimate lithology, gapped deconvolution or multiple subtraction to attenuate multiples and FX deconvolution to reduce random noise. Other tasks are suitable only for 'physical data', that is the not-enveloped Chirp or Boomer records: partial compensation of average anelastic absorption, wave equation migration and estimation of the $Q$ factor based on instantaneous frequency. Pinson et al. (2008) showed that the combined analysis of Chirp and Boomer data along the same profile achieves superior results because of the wider frequency band so obtained.

The traditional decision to record only the envelope of the Chirp signal, rather than its full waveform, is due to the otherwise difficult visual interpretation of this signal. The reason for this is the very limited bandwidth of Chirp recordings, which must be measured in octaves. Some recent system covers a frequency range between 1000 and 10,000 Hz, a little more than three octaves. Boomers' range covers 700–2000 Hz, nearly three octaves. Recently, commercial systems have been proposed that merge the two systems and cover a total range of 700–10,000 Hz (or even more), that is four octaves (de Oliveira Santos & Landim Dominguez 2019). Heavier sources, such as air guns or marine vibroseis, provide a much wider effective bandwidth, ranging from 4 to 128 Hz (and nominally even more), that is five octaves (and more). Of course, the resolution, penetration and cost of these systems are very different, but it is probably the deployment logistics that matter most. For offshore engineering purposes, we believe that merging Boomer and Chirp surveys is a promising prospect that needs further developments (see also Denich et al., 2021; Pinson et al., 2008). Mao and Stewart (2017) compared the different features of Boomer and Chirp surveys along the same profile, highlighting their complementarity.

## Sensitivity analysis

Mono-channel surveys are inherently weak with respect to noise or measurement errors, as they cannot rely on the stabilizing effect of averaging multiple sensors (see Bakulin et al., 2022, among others). Some partial sensitivity analysis has been carried out by Vesnaver and Baradello (2022a, 2022b, 2022c), which is summarized below, having in mind that more comprehensive studies are needed.

For the traveltime inversion, errors occur in the waveform picking due to both misinterpretations and interfering events.

If misspeaks and interferences are sparse, a median filtering along the profile enhances a lot the estimated Earth model (Vesnaver & Baradello, 2022a, 2022c). Random errors up to 0.1% of the traveltimes only introduce 30% errors in the estimated sediment velocity for a short offset of 2.5 m but decreases to 13% for an offset of 10 m. When the error exceeds 1%, instead, the instability is booming. As in our experimental test the traveltimes range from 10 to 30 ms, 0.1% errors correspond to about 20 μs, which approximate a standard sampling rate.

A critical parameter for Boomer surveys is the offset. When it is small (e.g. 2.5 m), errors of 1% due to cable feathering, sea waves or tension variations produce errors up to 2.6% in the estimated velocity and 2.8% in the thickness of the shallow sediments (Vesnaver & Baradello, 2022a). The sensitivity decreases when extending the offset to 10 m: thus, long offsets are recommended for the Boomer surveys.

Very challenging is the trade-off between the thickness and velocity of the shallow sediments, especially for Chirp data where we cannot count on the offset extension. In our approach, the joint traveltime inversion of primaries and various multiples provides a data redundancy with respect to the parameter number in the Earth model, making it overdetermined. In this way, an error in one input value may be partially averaged out by the inversion algorithm itself. This ambiguity may be reduced by introducing mathematical constraints, as linking the tomographic inversion to the Dix formula as a stabilizing reference and a lateral median filtering of the estimated parameters (Vesnaver & Baradello, 2022c).

The tomographic inversion is sensitive to the seawater velocity. Measuring it directly in the field, along the whole profile, would be a relevant technological implementation, as it would improve the estimation accuracy and stability of the other Earth model parameters.

## CONCLUSIONS

The processing of mono-channel Chirp or Boomer data presents major challenges in determining shallow seafloor lithologic parameters, such as P velocity, density and even anelastic absorption. We have shown that by picking and inverting multiple reflections, we can partially compensate for the information redundancy provided by different offsets in multichannel surveys. The amplitude trend of multiple reflections allows us to estimate the reflectivity of the seafloor and, based on traveltimes, the P velocity and thickness of the shallowest layer. This information is important for offshore engineers in the construction of piers and subsea pipelines, and for marine geologists in environmental studies.

The algorithms presented provide estimates that are quite stable in terms of trends but may be locally unstable. We, therefore, do not claim that they are bulletproof tools, but rather cost-effective alternatives for obtaining semi-quantitative estimates of shallow lithology that are preferable to extensive geotechnical drilling. The proposed workflow aims at a data-driven approach to reduce the processing costs and personal bias by physical criteria as much as possible.

## ACKNOWLEDGEMENTS

The marine seismic surveys were funded and carried out by OGS as part of the project 'Study of the geological and tectonic evolution of the Gulf of Trieste', led by Martina Busetti. Part of the data processing was performed using the Seismic Unix package (Cohen & Stockwell, 2013; Stockwell, 1999) and the SeisLab 3.02 software (Rietsch, 2015). We thank Claudio Bagaini and the other Reviewers for their hints and very constructive remarks.

## DATA AVAILABILITY STATEMENT

The synthetic data presented in the paper is provided upon request to the corresponding author (avesnaver@ogs.it).

## REFERENCES

Ackroyd, M.H. (1970) Instantaneous spectra and instantaneous frequency. *Proceedings IEEE*, 58, 141. https://doi.org/10.1109/proc.1970.7552.

Alkhalifah, T.A. (2014). *Full waveform inversion in an anisotropic world. Education tour series*. The Netherlands, Houten: EAGE, pp. 197. ISBN 9789462822023.

Alkhalifah, T.A., Almomin, A. & Naamani, A. (2021) Machine-driven earth exploration: artificial Intelligence in oil and gas. *The Leading Edge*, 40, 234–312. https://doi.org/10.1190/tle40040298.1.

Alves, D.P.V. & Mahiques, M.M. (2019) Deposition and sea-level evolution models for Upper Pleistocene/Holocene in the São Sebastião Channel (SE Brazilian coast) inferred from 5th order seismic stratigraphy. *Journal of South American Earth Sciences*, 93, 382–393. https://doi.org/10.1016/j.jsames.2019.05.012.

Bakulin, A., Neklyudov, D. & Silvestrov, I. (2022) Multiplicative random seismic noise caused by small-scale near-surface scattering and its transformation during stacking. *Geophysics*, 87, V419–V435. https://doi.org/10.1190/GEO2021-0830.1.

Baradello, L. (2014) An improved processing sequence for uncorrelated Chirp sonar data. *Marine Geophysical Research*, 35, 337–344. https://doi.org/10.1007/s11001-014-9220-1.

Barsottelli-Botelho, M.A. & Mesquita, L. (2015) Using GPR and high frequency seismic to locate under water buried pipes. In: *Near surface geoscience conference*. pp. We21P104. (Extended abstracts). EAGE, Bunnik, The Netherlands. https://doi.org/10.3997/2214-4609.201413812

Biondi, B.L. (2006) *3D seismic imaging* (pp. 247). Tulsa, USA: SEG. https://doi.org/10.1190/1.9781560801689.

Bull, J.M., Quinn, R. & Dix, J.K. (1998) Reflection coefficient calculation from marine high resolution seismic reflection (Chirp) data and application to an archaeological case study. *Marine Geophysical Research*, 20, 1–11. https://doi.org/10.1023/A:1004373106696.

Busetti, M., Babich, A. & Del Ben, A. (2020) Geophysical evidence of fluids emission in the Gulf of Trieste (North Adriatic Sea). *Memorie Descrittive della Carta Geologica d'Italia*, 105, 11–16, ISPRA (Rome, Italy).

Busetti, M., Volpi, V., Nicolich, R., Barison, E., Romeo, R., Baradello, L. et al. (2010) Dinaric tectonic features in the Gulf of Trieste (Northern Adriatic). *Bollettino di Geofisica Teorica ed Applicata*, 51(2–3), 117–128.

Busetti, M., Zgur, F., Vrabec, M., Facchin, L., Pelos, C., Romeo, R. et al. (2013) Neotectonic reactivation of Meso-Cenozoic structures in the Gulf of Trieste and its relationship with fluid seepings. In: *Proceedings of the 32nd Gruppo Nazionale di Geofisica della Terra Solida (GNGTS) Congress*. pp. 29–34.

Carcione, J.M. & Poletto, F. (2000) Sound velocity of drilling mud saturated with reservoir gas. *Geophysics*, 65, 646–651. https://doi.org/10.1190/1.1444761.

Cevatoglu, M., Bull, J.M., Vardy, M.E., Gernon, T.M., Wright, I.C. & Long, D. (2015) Gas migration pathways, controlling mechanisms and changes in sediment acoustic properties observed in a controlled sub-seabed $CO_2$ release experiment. *International Journal of Greenhouse Gas Control*, 38, 26–43. https://doi.org/10.1016/j.ijggc.2015.03.005.

Chapman, R.P. & Scott, H.D. (1964) Surface backscattering strengths measured over an extended range of frequencies and grazing angles. *Journal of the Acoustical Society of America*, 36(9), 1735. https://doi.org/10.1121/1.1919274.

Chen, J., Hu, G., Bu, Q., Wu, N., Liu, C., Chen, Q. et al. (2023) Elastic wave velocity of marine sediments with free gas: insights from CT-acoustic observations and theoretical analysis. *Marine and Petroleum Geology*, 150, 106169. https://doi.org/10.1016/j.marpetgeo.2023.106169.

Claerbout, J. (1985) *Imaging the Earth's interior*. Oxford, UK: Blackwell, pp. 233–234.

Cohen, J.K. & Stockwell, J.W., Jr. (2013) *CWP/SU: Seismic Un*x release 43R5, an open-source software package for seismic research and processing*. Golden, CO, USA: Center for Wave Phenomena, Colorado School of Mines. http://timna.mines.edu/cwpcodes/.

Conti, A., Stefanon, A. & Zuppi, G.M. (2002) Gas seeps and rock formation in the northern Adriatic Sea. *Continental Shelf Research*, 22, 2333–2344. https://doi.org/10.1016/S0278-4343(02)00059-6

Crocker, S.E. & Fratantonio, F.D. (2016) Characteristics of sounds emitted during high-resolution geophysical surveys. (NUWC-NPT Technical Report 12203, Newport, USA). pp. 266. https://apps.dtic.mil/sti/pdfs/AD1007504.pdf.

Denich, E., Vesnaver, A. & Baradello, L. (2021) Amplitude recovery and deconvolution of Chirp and Boomer data for marine geology and offshore engineering. *Energies*, 14, 5704. https://doi.org/10.3390/en14185704.

de Oliveira Santos, I. & Landim Dominguez, J.M. (2019) Mapeamento estratigráfico utilizando sísmica de alta resolução no trecho da futura Ponte Salvador-Itaparica, Bahia, Brasil. *Geologia USP, Série Cientifica*, 19(4), 85–98. https://doi.org/10.11606/issn.2316-9095.v19-150500.

Duchesne, M.J. & Bellefleur, G. (2007) *Processing of single-channel, high-resolution seismic data collected in the St. Lawrence estuary, Quebec*. Calgary, Canada: Geological Survey of Canada. Current Research, 2007-D1, pp. 11. https://doi.org/10.4095/223483

Dusart, J., Tarits, P., Fabre, M., Marsset, B., Jouet, G., Erhold, A. et al. (2022) Characterization of gas-bearing sediments in coastal environment using geophysical and geotechnical data. *Near Surface Geophysics*, 20, 478–493. https://doi.org/10.1002/nsg.12230.

Fomel, S. (2009) Adaptive multiple subtraction using regularized nonstationary regression. *Geophysics*, 74, V25–V33. https://doi.org/10.1190/1.3043447.

Fomel, S., Landa, E. & Taner, M.T. (2007) Post-stack velocity analysis by separation and imaging of seismic diffractions. *Geophysics*, 72, 1ND–Z100, https://doi.org/10.1190/1.2781533.

Gazdag, J. (1978) Wave equation migration with the phase-shift method. *Geophysics*, 43, 1342–1351. https://doi.org/10.1190/1.1440899.

Geletti, R., Del Ben, A., Busetti, M., Ramella, R. & Volpi, V. (2008) Gas seeps linked to salt structures in the Central Adriatic Sea. *Basin Research*, 20, 473–487. https://doi.org/10.1111/j.1365-2117.2008.00373.x.

Gordini, E., Falace, A., Kaleb, S., Donda, F., Marocco, R. & Tunis, G. (2012) Methane-related carbonate cementation of marine sediments and related macroalgal coralligenous assemblages in the Northern Adriatic Sea. In: Harris, P. T. & Baker, E. K. (Eds.) *Seafloor geomorphology as benthic habitats*. Amsterdam, The Netherlands: Elsevier, pp. 183–198. ISBN 978-0-12-3851 40-6.

Gordon, J., Gillespie, D., Potter, J., Frantzis, A., Simmonds, M.P., Swift, R. et al. (2003) A review of the effects of seismic surveys on marine mammals. *Marine Technological Society Journal*, 37, 16–34. https://doi.org/10.4031/002533203787536998.

Goswami, B.K., Weitemeyer, K.A., Minshull, T.A., Sinha, M.C., Westbrook, G.K. & Marín-Moreno, H. (2016) Resistivity image beneath an area of active methane seeps in the west Svalbard continental slope. *Geophysical Supplements to the Monthly Notices of the Royal Astronomical Society*, 207(2), 1286–1302. https://doi/org/10.1093/gji/ggw330.

Gutowski, M., Bull, J.M., Henstock, T.J., Dix, J.K., Hogarth, P., Leighton, T.G. et al. (2002) Chirp sub-bottom profiler source signature design and field testing. *Marine Geophysical Research*, 23, 481–492. https://resource.isvr.soton.ac.uk/staff/pubs/PubPDFs/Pub2555.pdf.

Helle, H.B., Pham, N.H. & Carcione, J.M. (2003) Velocity and attenuation in partially saturated rocks: poroelastic numerical experiments. *Geophysical Prospecting*, 51, 551–566. https://doi.org/10.1046/j.1365-2478.2003.00393.x.

Hite, D. & Fontana, P.M. (2007) Wide azimuth streamer acquisition: from field development to exploration applications, and back again. In: *10th international congress SBGF*. pp. 869–873. (Expanded abstracts). SEG (Houston, USA). https://doi.org/10.1190/sbgf2007-169.

Hovland, M. & Curzi, P. (1989) Gas seepage and assumed mud diapirism in the Italian central Adriatic Sea. *Marine and Petroleum Geology*, 6, 161–169. https://doi.org/10.1016/0264-8172(89)90019-6.

Huang, Y., Abubakar, A., Colombo, D., Gao, K., Kim, J.-H., Mantovani, M. et al. (2018) Introduction to special section: multiphysics imaging for exploration and reservoir monitoring. *Interpretation*, 6, SGi–SGii. https://doi.org/10.1190/int-2018-0713-spseintro.1.

Kim, G.Y., Narantsetseg, B., Kim, J.W. & Chun, J.H. (2014) Physical properties and micro-and macro-structures of gassy sediments in the inner shelf of SE Korea. *Quaternary International*, 344, 170–180. https://doi.org/10.1016/j.quaint.2014.01.049.

Landais, M., Mensch, T., Grenie', D. & Wombell, R. (2014) Broadband wide-azimuth towed streamer acquisition in West Africa. In: *84th SEG annual meeting*. pp. 138–142. (Expanded abstracts). SEG (Houston, USA). https://doi.org/10.1190/segam2014-0511.1.

Lin, L.F., Hsu, H.H., Liu, C.S., Chao, K.H., Ko, C.C., Chiu, S.D. et al. (2019) Marine 3D seismic volumes from 2D seismic survey with large streamer feathering. *Marine Geophysical Research*, 40, 619–633. https://doi.org/10.1007/s11001-019-09391-9.

Lin, R., Vesnaver, A., Böhm, G. & Carcione, J.M. (2018) Broad-band viscoacoustic Q-factor imaging by seismic tomography and instantaneous frequency. *Geophysical Journal International*, 214, 672–686. https://doi.org/10.1093/gji/ggy168.

Lin, R., Vesnaver, A., Böhm, G. & Carcione, J.M. (2022) Erratum of the paper: "broad-band viscoacoustic Q-factor imaging by seismic tomography and instantaneous frequency". *Geophysical Journal International*, 229, 898–899. https://doi.org/10.1093/gji/ggab526.

Mackenzie, K.V. (1981) Nine-term equation for sound speed in the oceans. *Journal of the Acoustical Society of America*, 70, 807–812. https://doi.org/10.1121/1.386920.

Maine, H. (1962) Common reflection point horizontal data stacking techniques. *Geophysics*, 27, 753–1027. https://doi.org/10.1190/1.1439118.

Mao, L. & Stewart, R.R. (2017) Near-surface imaging of the shallow sediments of Galveston Bay, Texas. In: *SEG annual meeting*. pp. 5958–5962. (Expanded abstracts). SEG (Houston, USA).https://doi.org/10.1190/segam2017-17794435.1.

McGee, T.M. (1995) High-resolution marine reflection profiling for engineering and environmental purposes. Part A: Acquiring analogue seismic signals. *Journal of Applied Geophysics*, 33(4), 271–285. https://doi.org/10.1016/0926-9851(95)90047-0.

Millero, F.J., C.T., Bradshaw, A. & Schleicher, K. (1980) A new high-pressure equation of state for seawater, Deep Sea Research Part A. *Oceanographic Research Papers*, 27, 255–264. ISSN 0198-0149. https://doi.org/10.1016/0198-0149(80)90016-3.

Moldoveanu, N., Nesladek, N. & Vigh, D. (2020) Wide-azimuth towed-streamer and large-scale OBN acquisition: a combined solution. In: *90th SEG annual meeting*. pp. 16–21. (Expanded abstracts). SEG (Houston, USA). https://doi.org/10.1190/segam2020-3425439.1.

Müller, C., Milkereit, B., Bohlen, T. & Theilen, F. (2002) Towards high-resolution 3D marine seismic surveying using Boomer sources. *Geophysical Prospecting*, 50, 517–526. https://doi.org/10.1046/j.1365-2478.2002.00335.x.

Müller, C., Woelz, S., Ersoy, Y., Boyce, J., Jokisch, T., Wendt, G. et al. (2009) Ultra-high-resolution 2D-3D seismic investigation of the Liman Tepe/Karantina Island archeological site (Urla/Turkey). *Journal of Applied Geophysics*, 68, 124–134. https://doi.org/10.1016/j.jappgeo.2008.10.015.

Peacock, K.L. & Treitel, S. (1969) Predictive deconvolution theory and practice. *Geophysics*, 34, 155–169. https://doi.org/10.1190/1.1440003.

Pecholcs, P.I., Lafon, S.K., Al-Ghamdi, T., Al-Shammery, H., Kelamis, P., Huo, S.X. et al. (2010) Over 40,000 vibration points per day with real-time quality control: opportunities and challenges. In: *SEG annual meeting*. pp. 111–115. (Expanded abstracts). SEG (Houston, USA). https://doi.org/10.1190/1.3513041.

Pecholcs, P.I., Al-Saad, R., Al-Sannaa, M., Quingley, J., Bagaini, C., Zarkidze, A. et al. (2012) A broadband full-azimuth seismic study from Saudi Arabia using a 100,000 channel recording system at 6 terabytes per day: acquisition and processing lessons learned. In: *SEG annual meeting*. pp. 1–5. (Expanded abstracts). SEG (Houston, USA). https://doi.org/10.1190/segam2012-0438.1.

Pinson, L.J.W., Henstock, T.J., Dix, J.K. & Bull, J.M. (2008) Estimating quality factor and mean grain size of sediments from high-resolution marine seismic data. *Geophysics*, 73, G19–G28. https://doi.org/10.1190/1.2937171

Plessix, R.E. (2008) Introduction: towards a full-waveform inversion. *Geophysical Prospecting*, 56, 761–762. https://doi.org/10.1111/j.1365-2478.2008.00736.x.

Riedel, M. & Theilen, F. (2001) AVO investigations of shallow marine sediments. *Geophysical Prospecting*, 49, 198–212. https://doi.org/10.1046/j.1365-2478.2001.00246.x.

Rietsch, E. (2015) *SeisLab 3.02. Release 15.09.21*. Natick, MA, USA: MathWorks©. https://www.mathworks.com/matlabcentral/fileexchange/53109-seislab-3-02

Robinson, E.A. & Treitel, S. (1967) Principles of digital Wiener filtering. *Geophysical Prospecting*, 15, 311–333. https://doi.org/10.1111/j.1365-2478.1967.tb01793.x.

Ruppel, C.D., Weber, T.C., Staaterman, E.R., Labak, S.J. & Hart, P.E. (2022) Categorizing active marine acoustic sources based on their potential to affect marine mammals. *Journal of Marine Science and Engineering*, 10, 1278. https://doi.org/10.3390/jmse10091278.

Russell, B., Hampson, D. & Chun, J. (1990) Noise elimination and the Radon transform. Part 1. *The Leading Edge*, 9(10), 18–23. https://doi.org/10.1190/1.1439677.

Saha, J.G. (1987) Relationship between Fourier and instantaneous frequency. In: *SEG annual meeting*. pp. 591–594. (Expanded abstracts). SEG (Houston, USA). https://doi.org/10.1190/1.1892041.

Schock, S.G. & LeBlanc, L.R. (1990) Chirp Sonar: new technology for sub-bottom profiling. *Sea Technology*, 31(9), 35–43.

Sills, G.C. & Wheeler, S.J. (1992) The significance of gas for offshore operations. *Continental Shelf Research*, 12(10), 1239–1250. https://doi.org/10.1016/0278-4343(92)90083-V.

Stockwell, J.W., Jr. (1999) The CWP/SU: Seismic Un*x package. *Computers & Geosciences*, 25, 415–419. https://doi.org/10.1016/S0098-3004(98)00145-9.

Sultan, N., Voisset, M., Marsset, T., Vernant, A.M., Cauquil, E., Colliat, J.L. et al. (2007) Detection of free gas and gas hydrate based on 3D seismic data and cone penetration testing: an example from the Nigerian Continental Slope. *Marine Geology*, 240(1–4), 235–255. https://doi.org/10.1016/j.margeo.2007.02.012.

Taner, M.T. & Koehler, F. (1969) Velocity spectra – digital computer derivation application of velocity functions. *Geophysics*, 34, 821–1041, https://doi.org/10.1190/1.1440058.

Taner, M.T., Koehler, F. & Sheriff, R.E. (1979) Complex seismic trace analysis. *Geophysics*, 44, 1041–1063, https://doi.org/10.1190/1.1440994.

Trobec, A., Busetti, M., Zgur, F., Baradello, L., Babich, A., Cova, A. et al. (2018)Thickness of marine Holocene sediment in the Gulf of Trieste (Northern Adriatic Sea). *Earth Science Data System*, 10, 1077–1092. https://doi.org/10.5194/essd-10-1077-2018.

Uge, M.A. & Alp, H. (2018) The comparison between two methods for Chirp seismic data processing. In: *EAGE annual meeting, Tu3ASM02*. (Extended abstracts). EAGE, Bunnik, The Netherlands. https://doi.org/10.3997/2214-4609.201802669

van der Sluis, A. & van der Vorst, H.A. (1987) Numerical solution of large, sparse linear systems arising from tomographic problems. In: Nolet, G. (Ed.) *Seismic tomography*. Hingham MA, USA: Reidel, pp. 49–83. https://doi.org/10.1007/978-94-009-3899-1_3.

Verbeek, N.H. & McGee, T.M. (1995) Characteristics of high-resolution marine reflection profiling sources. *Journal of Applied Geophysics*, 33(4), 251–269. https://doi.org/10.1016/0926-9851(95)90045-4.

Verschuur, D.J., Berkhout, A.J. & Wapenaar, C.P.A. (1992) Adaptive surface-related multiple attenuation. *Geophysics*, 57, 1166–1177. https://doi.org/10.1190/1.1443330.

Vesnaver, A. (1994) Towards the uniqueness of tomographic inversion solutions. *Journal of Seismic Exploration*, 3, 323–334.

Vesnaver, A. (2017) Instantaneous frequency and phase without unwrapping. *Geophysics*, 82, F1–F7. https://doi.org/10.1190/geo2016-0185.1.

Vesnaver, A., Accaino, F., Böhm, G., Madrussani, G., Pajchel, J., Rossi, G. et al. (2003) Time-lapse tomography. *Geophysics*, 68, 815–823. https://doi.org/10.1190/1.1581034.

Vesnaver, A. & Baradello, L. (2022a) Shallow velocity estimation by multiples for monochannel Boomer surveys. *Applied Sciences*, 12, 3046. https://doi.org/10.3390/app12063046.

Vesnaver, A. & Baradello, L. (2022b) Shallow velocities estimation by multiples in Boomer surveys. In: *83rd EAGE annual meeting*. (Expanded abstracts). EAGE, Bunnik, The Netherlands. https://doi.org/10.3997/2214-4609.202210195.

Vesnaver, A. & Baradello, L. (2022c) Tomographic joint inversion of direct arrivals, primaries and multiples for monochannel marine surveys, *Geosciences*, 12(6), 219. https://doi.org/10.3390/geosciences12060219.

Vesnaver, A., Busetti, M. & Baradello, L. (2021) Chirp data processing for fluid flow detection at the Gulf of Trieste (Northern Adriatic Sea). *Bulletin of Geophysics and Oceanography*, 62, 365–386. https://doi.org/10.4430/bgo00361.

Wiggins, W. (1988) Attenuation of complex water-bottom multiples by wave-equation-based prediction and subtraction. *Geophysics*, 53, 1527–1539. https://doi.org/10.1190/1.1442434.

Yilmaz, O. (2001) *Seismic data analysis*. Tulsa, USA: SEG, pp. 2065. ISBN: 978-1-56080-094-1 (print), 978-1-56080-158-0 (online).

Zecchin, M., Baradello, L., Brancolini, G., Donda, F., Rizzetto, F. & Tosi, L. (2008) Sequence stratigraphy based on high-resolution seismic profiles in the late Pleistocene and Holocene deposits of the Venice area. *Marine Geology*, 253, 3–4, 185–198. https://doi.org/10.1016/j.margeo.2008.05.010.

**How to cite this article:** Vesnaver, A. & Baradello, L. (2023) A workflow for processing mono-channel Chirp and Boomer surveys. *Geophysical Prospecting*, 71, 1387–1403. https://doi.org/10.1111/1365-2478.13389